

IMPEDANCE DATABASE FOR THE DIAMOND-II BOOSTER

R. Fielder*, R. Husain¹, F. Malinowski, S. Wang, Diamond Light Source, Oxfordshire, UK
¹also at John Adam Institute, University of Oxford, Oxfordshire, United Kingdom

Abstract

Boosters in synchrotron injector systems have traditionally had more relaxed designs than storage rings, and consequently impedance has not been considered an important factor in their designs. In 4th generation light sources like Diamond-II, it is desirable to increase the extracted charge per shot to reduce filling times and enable advanced injection schemes. As such, the vacuum chamber impedance becomes a significant design parameter. An impedance database has been created for the Diamond-II booster, using the same AT-style lattice concept as for the storage ring, to be used as input into particle tracking and other simulations. We present here an overview of the database, including details of significant components and current progress on engineering designs.

INTRODUCTION

The Diamond-II upgrade [1] to the existing Diamond synchrotron light source will provide a significant reduction in beam emittance. However, this comes at a cost of reduced dynamic aperture and lifetime, while more sensitive beam-lines require tighter constraints on acceptable disturbance to the stored beam. The Diamond-II booster [2, 3] has a more complex structure than the existing booster with stronger magnets, and is desired to produce higher charge per shot to reduce filling times. This makes beam impedance and collective effects much more significant concerns.

As previously reported [4, 5], we developed an impedance database for the Diamond-II storage ring, using an Accelerator Toolbox-like structure [6, 7] to allow easy updates and manipulation of data for tracking simulations. We have produced a similar database using the same principles for the Diamond-II booster ring, and present here an overview of the main contributions.

BOOSTER OVERVIEW

The Diamond-II booster will occupy the same tunnel as the existing booster, and will therefore have the same race-track layout consisting of two straights for injection and extraction, joined by two arcs. Each straight also contains one 5-cell RF cavity. The arcs consist of an 11.5 mm radius stainless steel vacuum pipe, with alternating BPM or pump and bellows assembly after each dipole. The layout of part of the booster ring is shown in Fig. 1.

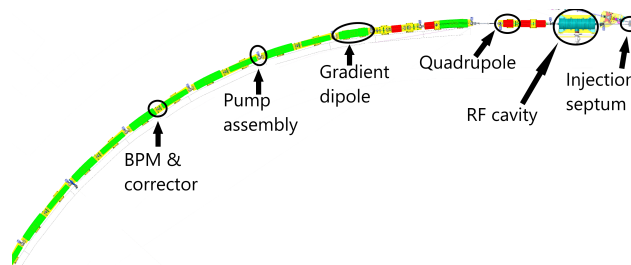


Figure 1: Top-down view of booster showing significant parts in portion of arc and injection straight.

GEOMETRIC IMPEDANCE

Simulation Parameters

Geometric and resistive wall contributions are considered separately, making it easier to test the effects of changing materials or component geometry independently without needing to re-run full simulations every time. The geometric impedance is calculated using the CST Studio [8] wake-field solver, using a 0.5 mm bunch length and 300 mm wake length, the same parameters as used for the short-range wake in the storage ring. Although bunch length in the booster varies significantly during the ramp [9], the s-band bunchlets from the electron gun provide the shortest bunch length ($\sigma = 1.5$ mm), so a short drive bunch is still required for simulations to see the high frequency behaviour. Injection into the booster occurs at 100 MeV, and the energy is ramped up to 3.5 GeV at extraction where the equilibrium bunch length becomes 12 mm due to emission of synchrotron radiation. Except for the cavities, all geometric and resistive wall impedance is summed together, weighted by beta function, to provide a total lumped impedance for each plane.

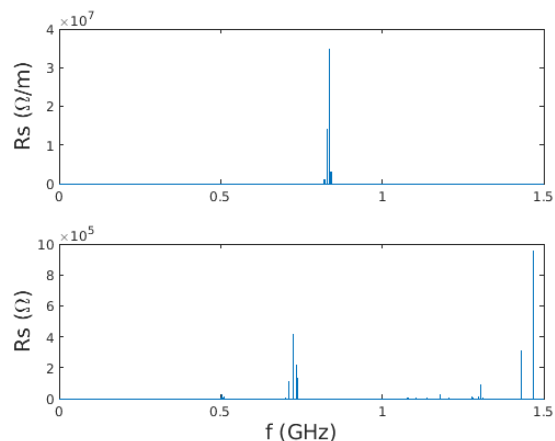


Figure 2: Transverse (top) and longitudinal (bottom) higher-order modes for booster cavities.

* richard.fielder@diamond.ac.uk

RF Cavities

As with the storage ring impedance, the RF cavities' large size and strong resonances makes them unfeasible to simulate wakefields directly with the required resolution. These are instead included in tracking simulations using high-order modes (HOMs) calculated with the CST Studio eigenmode solver, shown in Fig. 2.

Pump Assembly

Pump assemblies consist of a pumping cross with an internal bellows cartridge. Several bellows designs were investigated, and one based on the APS [10] bellows design was chosen due to its better mechanical performance, although with somewhat worse impedance. The geometric impedance of the pump assembly is shown in Fig. 3.

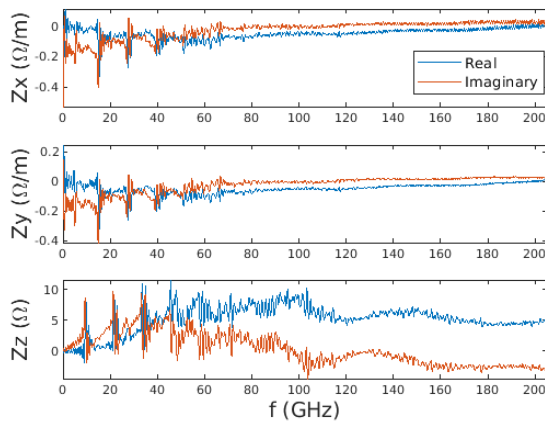


Figure 3: Geometric impedance of booster pump and bellows assembly.

Valves

There are a total of eight vacuum valves in the booster ring. Each RF cavity has valves upstream and downstream to allow the cavity to be isolated from the rest of the ring, with further valves approximately 1/3 and 2/3 of the way around each arc. A standard VAT [11] valve design is used.

Screens

Diagnostic fluorescent screens are present in each straight. These are retracted from the beam pipe when not in use, with a matching cylindrical pipe section inserted in their place. Since gaps must be present at the edges to allow this movement, the matching cannot be perfect and so they still present some impedance to the beam. The impedance of the screen assembly with screens retracted and matching section in place is shown in Fig. 4.

Kickers

There are four pulsed kicker magnets in the booster, one for injection and three for extraction. These use a window-frame instead of the C-shape of the existing kickers, with tapers added extending from the incoming beam pipe to

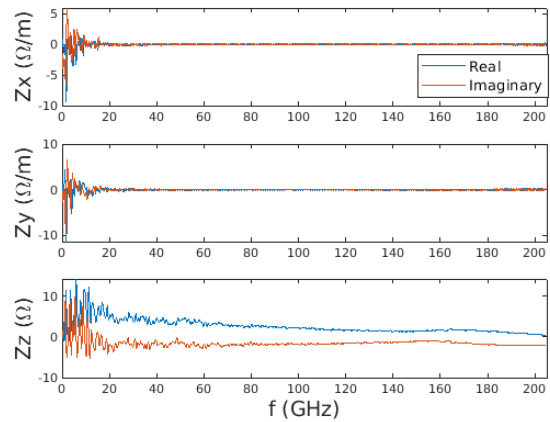


Figure 4: Geometric impedance of booster screen assembly.

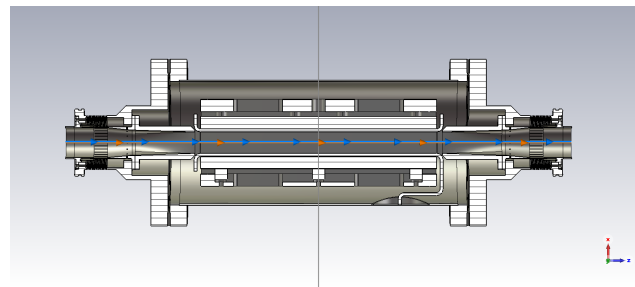


Figure 5: Top down view of kicker vessel.

almost touch the ferrite, along with other efforts to reduce discontinuities. The internal parts of the magnet consist of ferrite blocks above and below the beam with copper conductors in the horizontal. Limitations in some codes mean only one material can be defined for all planes at a given location, so ferrite is used to ensure the worst case is covered. A cutaway view of the kicker assembly is shown in Fig. 5, and the geometric impedance is shown in Fig. 6.

Since bare ferrite has extremely large resistive wall impedance, coating with a conductive material is planned to be used. However, such coatings can reduce the perfor-

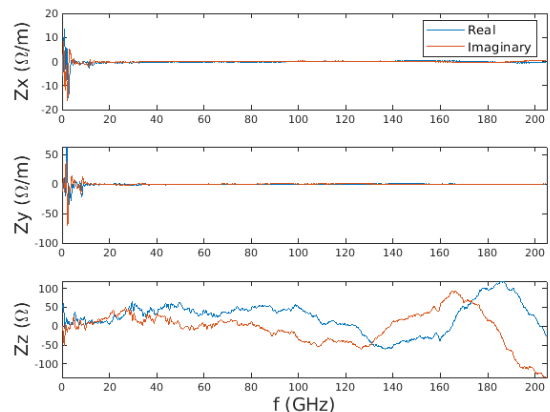


Figure 6: Geometric impedance of booster kicker.

mance of the kicker by shielding the beam from the pulsed magnetic field, and can also suffer potentially damaging heating from induced eddy currents. Investigations of coating materials and thickness are still ongoing; in this paper a uniform coating of 100 nm titanium nitride is assumed. The possibility of striped or other non-uniform coatings is also under consideration.

Flanges

Unlike the storage ring, the booster flanges will not have true zero-gap, and instead will use a half-spigot design with a small gap close to the beam which opens to a larger gap further from the beam. Studies of the effect of different flange dimensions on single bunch instabilities and on manufacturing capabilities have been carried out, and tolerances have been defined to ensure that the gap remains $< 200 \mu\text{m}$ in all cases. The effect of changing flange gaps on summed short-range wake potential is shown in Fig. 7.

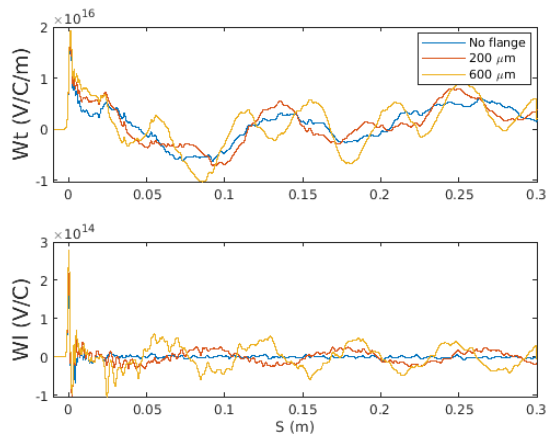


Figure 7: Total wake potential for booster with different flange dimensions.

RESISTIVE WALL

The resistive wall contribution was calculated using the ImpedanceWake2D code [12]. The materials used, including different radius vacuum pipes, are shown in Table 1. Two alumina ceramic breaks are present, one in each arc, to terminate eddy currents generated during the energy ramp. Since this is calculated analytically, computing time is not a problem and so the resistive wall wake is calculated up to 5,000 m, to cover both single bunch and multibunch effects. Total real and imaginary resistive wall impedance is shown in Fig 8.

SUMMARY AND FUTURE WORK

The total loss and kick factors for the significant components in the booster ring are shown in Table 2. The resistive wall is by far the most significant contribution in the transverse planes, mainly due to the ceramic breaks and kicker ferrite. In the longitudinal, the flanges are the most significant component from geometric wakes, although the RF

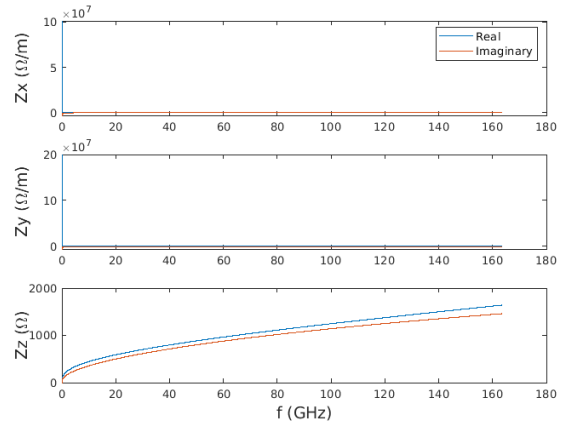


Figure 8: Total resistive wall impedance (top: horizontal, middle: vertical, bottom: longitudinal).

Table 1: Table of Materials for Resistive Wall Impedance

Material	Length (m)	Percentage
Stainless steel (18.3 mm)	18.27	11.15
Stainless steel (11.5 mm)	144.41	88.14
Ferrite	1.15	0.70
Alumina	0.02	0.01

cavity HOMs have a larger influence. Results of particle tracking using this impedance database are reported in [13].

A few components such as injection and extraction septa remain to be designed, while investigation of kicker vessels and ferrite coating are currently a focus. Simulation of long range geometric wakes for multibunch collective effects has begun; testing to determine the required simulation parameters is being carried out in parallel with similar work on the storage ring [14].

Table 2: Table of Total Loss and Kick Factors for Main Booster Components Calculated for a 12 mm Bunch

Component (Number present)	x (V/pC/mm)	y (V/pC/mm)	z (V/pC)
Screens (2)	-0.020	-0.015	0.048
Valves (8)	-0.001	-0.006	0.000
BPM (Str.) (4)	-0.003	-0.000	0.000
BPM (Arc) (44)	-0.021	-0.034	0.013
Pumps (57)	-0.015	-0.009	0.003
Kickers (4)	-0.014	-0.010	0.522
Cavity tapers (2)	-0.015	-0.002	0.118
Flange (Str.) (41)	-0.036	-0.036	0.700
Flange (Arc) (183)	-0.287	-0.287	4.520
Resistive wall	-3.588	-7.192	1.658
Total	-3.985	-7.595	7.578

REFERENCES

- [1] Diamond-II Technical Design Report, Diamond Light Source, <https://www.diamond.ac.uk/Diamond-II.html>, Accessed: 2024-04-09.
- [2] I. P. S. Martin *et al.*, “Progress with the Booster Design for the Diamond-II Upgrade”, in *Proc. IPAC’21*, Campinas, Brazil, May 2021, pp. 286–289.
doi:10.18429/JACoW-IPAC2021-MOPAB071
- [3] I. P. S. Martin *et al.*, “Beam Dynamics Studies for the Diamond-II Injector”, in *Proc. IPAC’22*, Bangkok, Thailand, Jun. 2022, pp. 2708–2711.
doi:10.18429/JACoW-IPAC2022-THPOPT049
- [4] R. T. Fielder and T. Olsson, “Construction of an Impedance Model for Diamond-II”, in *Proc. IPAC’21*, Campinas, Brazil, May 2021, pp. 455–458.
doi:10.18429/JACoW-IPAC2021-MOPAB127
- [5] D. Rabusov, R. Fielder, and S. Wang, “Analysis of single-bunch instabilities for Diamond-II”, in *Proc. IPAC’23*, Venice, Italy, May 2023, pp. 3550–3553.
doi:10.18429/JACoW-IPAC2023-WEPL184
- [6] A. Terebilo, “Accelerator Modeling with MATLAB Accelerator Toolbox”, in *Proc. PAC’01*, Chicago, IL, USA, Jun. 2001, paper RPAH314, pp. 3203–3205.
- [7] “Accelerator Toolbox”, ATCOLLAB, version 2.0, <https://atcollab.github.io/at/>, Accessed: 2024-05-02
- [8] CST Studio Suite, <https://www.3ds.com/products/simulia/cst-studio-suite>, Accessed: 2024-05-01
- [9] R. Husain, P. Burrows, R.T. Fielder, and I.P.S. Martin, “Evolution of Equilibrium Parameters Ramp Including Collective Effects in the Diamond- II Booster”, in *Proc. FLS’23*, Luzern, Switzerland, Aug.-Sep. 2023, pp. 120–123.
doi:10.18429/JACoW-FLS2023-TU4P19
- [10] J. Jones, S. Sharma, D. Bromberek, and J. Howell, “APS SR Flexible Bellows Shield Performance”, in *Proc. PAC’99*, New York, NY, USA, Mar. 1999, paper THP62, pp. 3095–3097.
- [11] VAT Group AG, <https://www.vatvalve.com/>, Accessed: 2024-04-29
- [12] ImpedanceWake2D, <https://twiki.cern.ch/twiki/bin/view/ABPCComputing/ImpedanceWake2D>, Accessed: 2024-04-29.
- [13] R. Husain, S. Wang, P. Burrow, R. Fielder, I. Martin, “Studies of single bunch and multi-bunch beam instabilities in the Diamond-II booster”, presented at the IPAC’24, Nashville, USA, May 2024, paper TUPG18, this conference.
- [14] R. Fielder, D. Rabusov, S. Wang, “Updates to the impedance database for the Diamond-II storage ring”, presented at the IPAC’24, Nashville, USA, May 2024, paper THPC50, this conference.